Die-Attached Versus Die-Detached Resin Injection Chamber for Pultrusion

D. R. Palikhel · J. A. Roux · A. L. Jeswani

Abstract Resin injection pultrusion is an efficient and highly automated continuous process for high-quality, low-cost, high-volume manufacturing of composites. The main objective of this study is to explore the "attached-die configuration" and "detached-die configuration" for improving the resin injection pultrusion process. In this work the impact of pull speed on complete wet out of the reinforced fiber is investigated for attached-die and detached-die resin injection pultrusion with various chamber length considerations. A 3-D finite volume technique was applied to simulate the liquid resin flow through the fiber reinforcement in the injection pultrusion process. This work explores the resin injection pressure needed to achieve complete wet out and the corresponding maximum pressure inside the resin injection chamber so as to improve injection chamber design to keep the pressure within the injection chamber within reasonable constraints for different pull speeds.

Keywords Pultrusion · Resin injection · Pull speed · Compression ratio

1 Introduction

Composite materials are engineered materials formed by the artificial combination of two or more materials differing in form or composition in macroscale so as to attain mechanical properties that the individual components by themselves cannot attain. Composites have many applications which can be generally summarized as structural applications, electronic applications, thermal applications, electrochemical applications, environmental applications and biomedical applications. One of the major cost factors in the manufacturing of polymer composites is the cost of fabrication. Pultrusion is a continuous, cost-effective method for manufacturing composite structural components with constant cross sections. The

D. R. Palikhel · J. A. Roux (✉)
Department of Mechanical Engineering, University of Mississippi, Oxford, MS 38677, USA
e-mail: meroux@olemiss.edu

A. L. Jeswani
OSRAM SYLVANIA, Danvers, MA, USA

components of a pultrusion machine are creel, resin wet out station, forming dies, heated metal die, puller mechanism, and cutoff saw as shown in the Fig. 1. Resin injection pultrusion is an efficient process for high-quality, low-cost, high-volume manufacturing of fiber reinforced polymeric composites.

Process models can be used to overcome the limitations imposed by the lack of adequate sensors to monitor the key processing variables. The models can also be used in a predictive control strategy which provides the ability to view the forecasted behaviors of the process. Hence, model based design and improvement are desirable and necessary. Overall, simulation models are very useful and can be effectively used to design the injection pultrusion process and to improve productivity and reduce cost.

Significant research works have been done on experimental and numerical analyses of the resin injection pultrusion process. These consist of the research at the University of Mississippi [1–5], Washington University [6–8], the University of Minnesota [9], and the Ohio State University [10, 11]. Liu [12] developed 2-D and 3-D finite element/nodal volume techniques to simulate the resin flow through the fiber reinforcement during the injection pultrusion process. Liu [13] also developed transient and iterative finite element/nodal volume methods to predict the steady-state flow front location; numerical performance from these models were investigated for low pull speed, injection pressure and variation of permeability. Srinivasagupta et al. [6] developed a rigorous model-based design algorithm and using a validated 3D dynamic processing model, developed integrated procedures for model-based design incorporating economic, controllability, environmental, and quality objectives.

Mustafa, Khomami and Kardos [8] developed a 3-D flow simulation model for injection pultrusion process which was used to demonstrate the effect of fiber pull speed, reinforcement anisotropy, and taper of the die on the product quality. A simple pulling-force model was developed and integrated with the simulation model. To account for the tapering of the injection chamber, the source term is crucial in the pressure equation for correct injection pressure assessment, but they omitted the source term in the pressure equation in their analysis. Rahetakar and Roux [3] developed a 2-D finite volume method to predict the resin

Fiber Reinforcement Creel
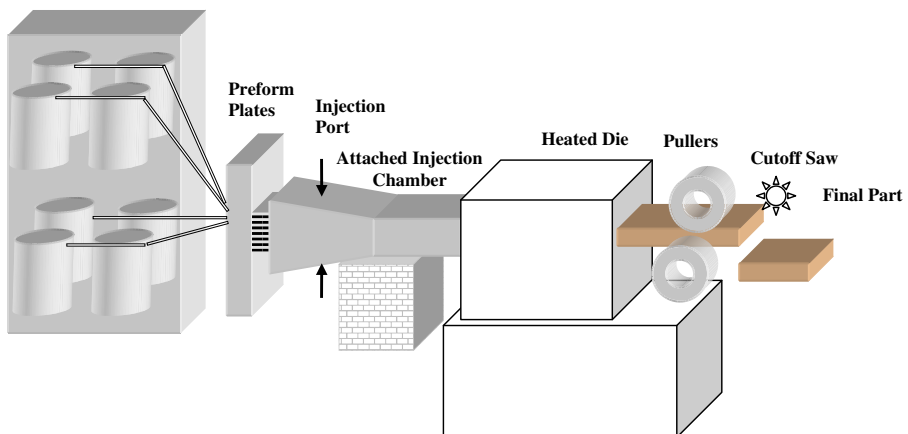
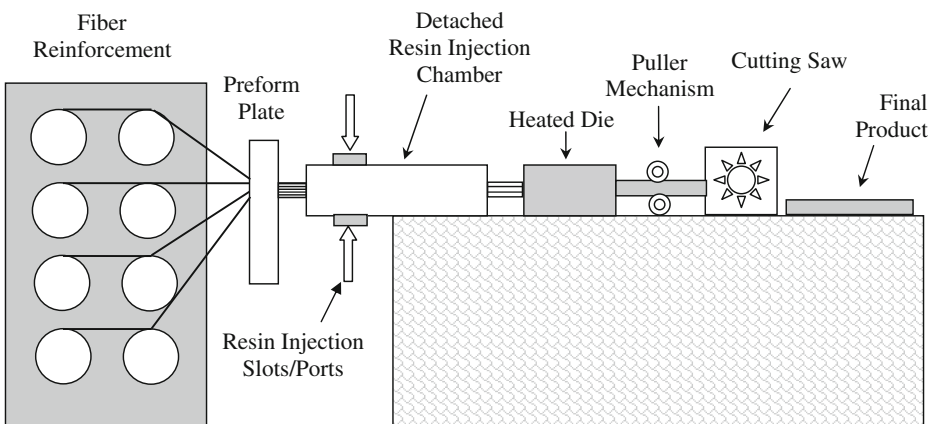Fig. 1 Schematic of die-attached resin injection pultrusion

pressure field, resin velocity field and resin moving flow front location. They modeled and analyzed the slot injection port system developed from the 2-D model.

Jeswani and Roux [1] developed a 3-D finite volume technique to simulate the flow of resin through the fiber reinforcement (E-glass rovings) in the injection pultrusion process. They predicted the impact of the tapering of the injection chamber walls on the minimum injection pressure necessary to achieve complete wet out. They studied two injection chamber configurations (a) die-attached (Fig. 1) and (b) die-detached (Fig. 2) configurations and predicted the minimum injection pressure necessary to attain complete wet out, location of the liquid resin flow front, and the pressure field. Their work showed that the resin injection chamber interior pressures can reach dangerously high levels.

The goal of the present work is to investigate the resin injection pressure needed to achieve complete wet out, the corresponding maximum pressure inside the resin injection chamber and to predict the resin flow front location by varying the length of injection chamber for different processing parameters in the "attached-die configuration" and "detached-die configuration" of the resin injection pultrusion process. The processing parameters explored are pull speed, the injection chamber length, and compression ratio. In this work, analysis will be conducted to predict the impact of variation of injection chamber lengths and pull speeds. A broader range of operating conditions is presented in this work than that found in previous works [5, 6, 9]. None of the previous researchers discussed above have analyzed the impact of varying the length of the tapered resin injection chamber coupled with the "detached-die configuration" for the resin wet out process.

2 Statement of the Problem

The effect of resin injection pressure on the wet out process is a very important aspect in the pultrusion process as the wet out of the fiber reinforcement affects the mechanical quality of the final composite. Wet out can be achieved with different injection pressures, design and processing configurations; but the main focus here is to determine the successful pressure operating conditions so that the process is economical and efficient and functions within safe


Fig. 2 Schematic of die-detached resin injection pultrusion

injection pressures and safe maximum pressures within the injection chamber. The tapered shape of the injection chamber has a strong impact on the wet out process and the injection pressure required for the complete wet out as the compression of the fiber matrix results in a change (increase) of the fiber volume fraction and a resulting decrease in the permeability as the fiber matrix progresses along the longitudinal (x) direction into the tapered resin injection chamber.

The regions and the geometry of the injection chamber are illustrated in the Fig. 3. The injection chamber is divided into two primary regions: Region I and Region II. In Region I, the injection chamber walls are tapered and the liquid resin injection slots are located here. Short chamber lengths with different processing parameters and compression ratios are investigated so as to reduce the injection chamber internal pressures and to achieve complete wet out at reduced minimum injection pressures [5]. In this study the total (Region I plus Region II) chamber lengths considered are 0.15 m, 0.20 m, and 0.30 m; this was varied by changing the length of Region I, while Region II was set to a constant length of 0.05 m. A schematic of the computational domain of the injection chamber for the present analysis is shown in Fig. 4. This figure illustrates the side and the top views of the injection chamber, axes of the domain, height and width of the front and outflow boundaries, injection slot position (x_{IS}), the taper angle (α), and the lengths of Region I (L_{IC}) and Region II (L_D) considered for the analysis.

Here (Fig. 4) H_{IC} and W_D represent the height and width of the front boundary of the injection chamber in Region I, and H_D and W_D represent the height and width of the exit portion of Region II. In the detached-die configuration, a gap space of 0.005 m is placed at the end of Region II of the computational domain between the resin injection chamber exit and outflow boundary (die entrance) as shown in Fig. 4. This configuration gap acts as a pressure release mechanism where the fiber/resin system perimeter is subjected to atmospheric pressure in this gap region beyond the exit of the injection chamber. Compression ratio, CR, is the ratio of the height of the injection chamber at the front boundary in Region I to the height of the injection chamber at the exit boundary in Region II; CR is given by CR=H_{IC}/H_D.
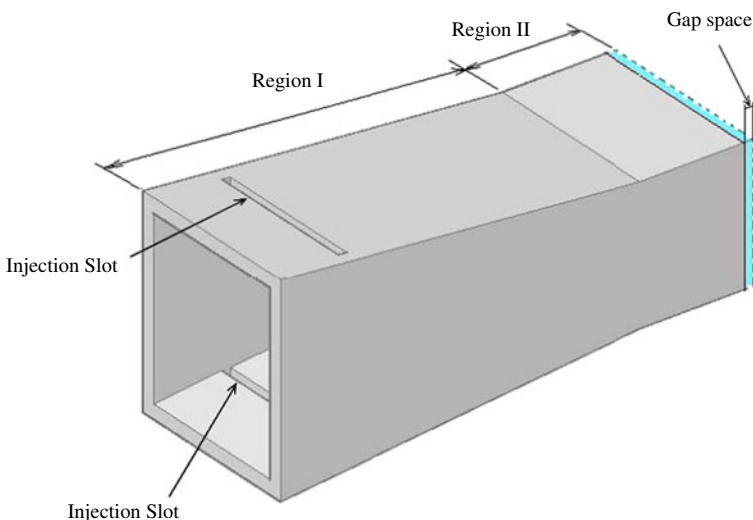
Fig. 3 Physical description of tapered injection chamber

(a) In *xy* Plane (Side View)

(b) In *xz* Plane (Top View)
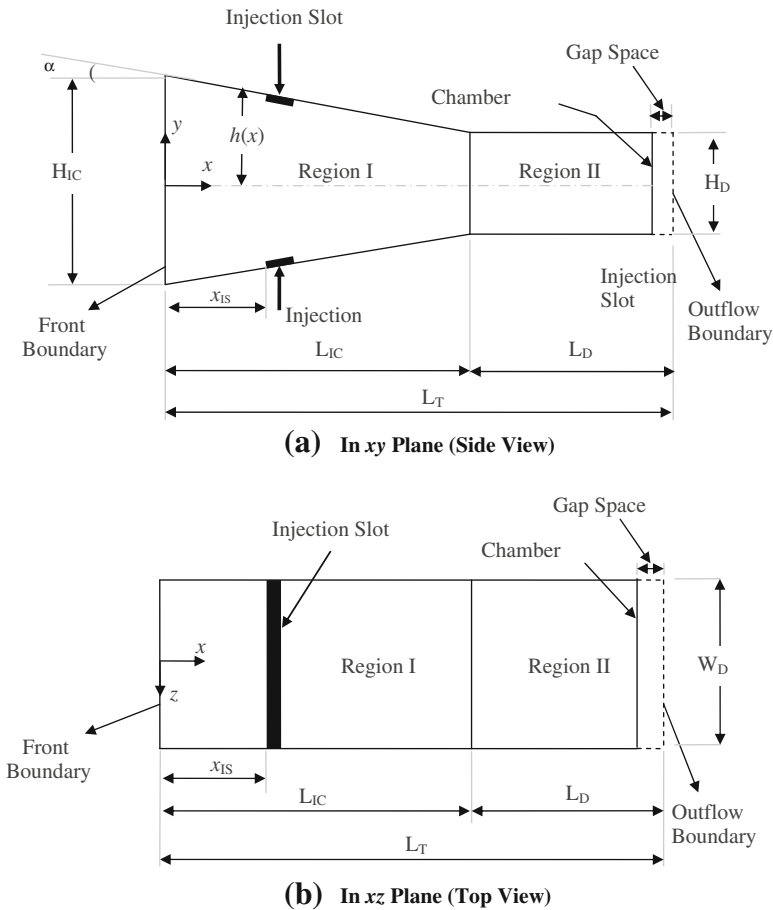
Fig. 4 Sketch of the computational domain for the die-detached resin injection chamber (not to scale)

3 Analysis

3.1 Permeability Model

Permeability indicates resistance to the flow of resin through the fiber bed; the higher the permeability the lower is the resin flow resistance and vice versa. The current study employs the Gutowski et al. [14] permeability model. Resistance to resin flow in the transverse directions (y and z) is higher than the flow resistance in the longitudinal direction (x) due to the fiber matrix system interference being higher in the transverse directions and also due to the orthotropic nature of the fiber matrix system arrangement. Gutowski et al. [14] have proposed a model in which the permeability of the rovings in the longitudinal direction is the same as the Kozeny-Carman model [15] defined by the following expression

$$K_{11} = \frac{R_f{}^2}{4k} \frac{\left(1 - V_f\right)^3}{V_f{}^2} \tag{1}$$

but the permeabilities in the transverse directions are given by

$$K_{22} = K_{33} = \frac{R_f^2}{4k'} \frac{\left(\sqrt{\frac{V_a'}{V_f}} - 1\right)^3}{\left(\frac{V_a'}{V_f} + 1\right)} \tag{2}$$

where K_{11}, $K_{22,}$ K_{33} are the components of permeability in the x, y, and z directions, respectively, k is the Kozeny constant, R_f is fiber radius (R_f=15 μm for glass fibers), and V_f is the local fiber volume fraction where V_a' and k' are empirical parameters; here [14] k=1.4, k'=0.20, and $V_a' = 0.907$ for hexagonal fiber packing of the fiber roving.

3.2 Fiber Volume Fraction and Porosity

The fiber volume fraction (V_{fo}) of the manufactured composite material is defined as the volume fraction of reinforcement fiber in the final composite. Whereas the fraction of non-fiber volume in the final composite is defined by the porosity, φ. The local fiber volume fraction at different points in the longitudinal coordinate (x) in the injection chamber is expressed as V_f. For Region I the injection chamber is tapered, thus the volume of fiber remains constant but the cross section decreases continuously along the longitudinal coordinate x, hence the porosity, φ, and local fiber volume fraction, ($V_f(x)$) become functions of the longitudinal coordinate x; the local fiber volume fraction, $V_f(x)$, increases with an increasing x dimension in Region I.

The local fiber volume fraction, $V_f(x)$, is a minimum at the front of the injection chamber. It increases along the axial coordinate, and achieves a maximum value (V_{fo}) at the end of Region I. In Region II the local fiber volume fraction (V_{fo}) is constant since there are no tapered walls of the injection chamber in Region II. So the local fiber volume fraction at the end of Region I and throughout Region II are the same as the fiber volume fraction of the final composite, i.e., $V_f(x)$=V_{fo} in Region II. The relationship between local porosity $\varphi(x)$ and local fiber volume fraction $V_f(x)$ is given by

$$\varphi(x) = 1 - V_f(x) \tag{3}$$

The permeabilities depend on local fiber volume faction which in turn is a function of x, thus the permeabilities are also a function of x in Region I. $V_f(x)$ is expressed as

$$V_f(x) = V_{fo}\left(\frac{H_D}{2h(x)}\right) \tag{4a}$$

where $h(x)$ as shown in Fig. 4 is given by

$$h(x) = -\left(\frac{H_{IC} - H_D}{2L_{IC}}\right)(x - L_{IC}) + \frac{H_D}{2} \tag{4b}$$

3.3 Governing Equations for Region I and Region II of the Injection Chamber

The continuity equation for flow of resin through the fiber matrix is given by

$$\frac{\partial(u\varphi)}{\partial x} + \frac{\partial(v\varphi)}{\partial y} + \frac{\partial(w\varphi)}{\partial z} = 0 \tag{5}$$

where,

$$u = U - \frac{K_{11}}{\mu\varphi}\frac{\partial P}{\partial x}; \quad v = V - \frac{K_{22}}{\mu\varphi}\frac{\partial P}{\partial y}; \quad w = -\frac{K_{33}}{\mu\varphi}\frac{\partial P}{\partial z} \tag{6}$$

Here u, v, and w are the Darcy [16] components of resin velocity in three co-ordinate directions, φ is the porosity, and U (pull speed) and V are the velocity components of the fiber reinforcement in the x, and y directions respectively. $-\frac{K_{11}}{\mu\varphi}\frac{\partial P}{\partial x}$, $-\frac{K_{22}}{\mu\varphi}\frac{\partial P}{\partial y}$, and $-\frac{K_{33}}{\mu\varphi}\frac{\partial P}{\partial z}$ are the three components of the liquid resin velocity relative to the moving reinforcement. K_{11}, K_{22}, K_{33} are the components of the permeability and μ is the viscosity ($\mu \sim 0.75$ Pa·s for a phenolic resin system) of the resin. For Region I, substituting u, v, and w into the continuity equation (Eq. 5) yields

$$\frac{\partial}{\partial x}\left(U\varphi - \frac{K_{11}}{\mu\varphi}\frac{\partial P}{\partial x}\varphi\right) + \frac{\partial}{\partial y}\left(V\varphi - \frac{K_{22}}{\mu\varphi}\frac{\partial P}{\partial y}\varphi\right) + \frac{\partial}{\partial z}\left(-\frac{K_{33}}{\mu\varphi}\frac{\partial P}{\partial z}\varphi\right) = 0 \tag{7}$$

On simplifying Eq. 7, the pressure equation becomes

$$\frac{\partial}{\partial x}\left(\frac{K_{11}}{\mu}\frac{\partial P}{\partial x}\right) + \frac{\partial}{\partial y}\left(\frac{K_{22}}{\mu}\frac{\partial P}{\partial y}\right) + \frac{\partial}{\partial z}\left(\frac{K_{33}}{\mu}\frac{\partial P}{\partial z}\right) = \frac{\partial(U\varphi)}{\partial x} + \frac{\partial(V\varphi)}{\partial y} \tag{8}$$

The fiber velocity in the y-direction (V) is given by Eq. 9 below in terms of taper angle (α), fiber velocity in the x-direction (U), and position in the y-direction

$$V = -U\left(\frac{y}{h(x)}\right)\tan\alpha \tag{9}$$

where the vertical distance y varies according to the relation $-h(x) \le y \le h(x)$ and $h(x)$ is given earlier in Eq. 4b. Substituting the fiber velocity V from Eq. 9 into Eq. 8 results in the following equation

$$\frac{\partial}{\partial x}\left(\frac{K_{11}}{\mu}\frac{\partial P}{\partial x}\right) + \frac{\partial}{\partial y}\left(\frac{K_{22}}{\mu}\frac{\partial P}{\partial y}\right) + \frac{\partial}{\partial z}\left(\frac{K_{33}}{\mu}\frac{\partial P}{\partial z}\right) = U\left\{\frac{\partial\varphi}{\partial x} - \frac{\varphi}{h(x)}\tan\alpha\right\} \tag{10}$$

Equation 10 is the governing pressure equation for Region I. The right-hand side of Eq. 10 acts like a source term for pressure due to the tapered walls of the injection chamber in Region I. Compression produces a pressure rise in the liquid resin due to the tapering of the injection chamber walls. In Region II of the injection chamber the walls are not tapered (α=0) so the fiber velocity in the y-direction (V=0) is equal to zero. Since U and φ are constant in Region II, the term $\partial\varphi/\partial x$ vanishes and Eq. 10 simplifies to the following equation without a source term for Region II

$$\frac{\partial}{\partial x}\left(\frac{K_{11}}{\mu}\frac{\partial P}{\partial x}\right) + \frac{\partial}{\partial y}\left(\frac{K_{22}}{\mu}\frac{\partial P}{\partial y}\right) + \frac{\partial}{\partial z}\left(\frac{K_{33}}{\mu}\frac{\partial P}{\partial z}\right) = 0 \tag{11}$$

3.4 Boundary Conditions

The governing pressure equations for Region I and Region II (Eqs. 10 and 11) are second order partial differential equations. So six spatial boundary conditions, two in each coordinate direction are required for solution for the pressure field. There is no penetration of resin through the wall of the injection chamber, thus the boundary conditions

along the chamber walls are established by setting to zero the normal component to the chamber wall of the resin resultant velocity. At the outlet of the injection chamber, the velocity of the resin in the x-direction is equal to the fiber velocity [12, 16] in the x-direction ($u=U$). The computational domain is symmetric about the xy and xz-planes. Hence, only a quarter of the computational domain was necessary to be modeled. Therefore the boundary conditions were suitably defined to simulate the resin flow in a quarter of the computational domain; this reduces the number of computational nodes significantly. The boundary conditions corresponding to the quarter domain for the "attached-die" injection chamber configuration are given by

$$P = P_{atm} \quad \text{at } x = 0 \tag{12}$$

$$P = P_{Inj} \quad \text{at injection slot } (x = x_{IS}) \tag{13}$$

$$\frac{K_{11}}{\mu\varphi} \frac{\partial P}{\partial x} \sin\alpha + \frac{K_{22}}{\mu\varphi} \frac{\partial P}{\partial y} \cos\alpha = 0 \quad \text{at } y = h(x)(\text{Region I}) \tag{14}$$

$$\frac{\partial P}{\partial y} = 0 \quad \text{at } y = 0(\text{Region I}) \tag{15}$$

$$\frac{\partial P}{\partial z} = 0 \quad \text{at } z = 0 \text{ and at } z = W_D/2(\text{Region I and Region II}) \tag{16}$$

$$\frac{\partial P}{\partial y} = 0 \quad \text{at } y = 0 \text{ and at } y = H_D/2(\text{Region II}) \tag{17}$$

$$\frac{\partial P}{\partial x} = 0 \quad \text{at } x = L_T \tag{18}$$

For the "detached-die" injection chamber configuration, there is a gap between the resin injection chamber and the heated die inlet. At the end of the injection chamber (Region II) a gap of 0.005 m in length is modeled at the circumferential surface area of the resin/matrix system in this gap space; this gap circumferential surface is subjected to an atmospheric pressure boundary condition in the region L_T – 0.005 m$<x \leq L_T$ (see Figs. 3 and 4). Thus boundary conditions for Region I are same as that for the attached-die configuration (Eq. 12 to Eq. 15), whereas, the boundary conditions for the detached-die configuration for Region II are given by the following equations

$$\frac{\partial P}{\partial y} = 0 \quad \text{at } y = H_D/2 \text{ and } L_{IC} \leq x \leq L_T - 0.005\text{m (Region II)} \tag{19}$$

$$P = P_{atm} \quad \text{at } y = H_D/2 \text{ and } L_T - 0.005\text{m} < x \leq L_T \text{ (Region II)} \tag{20}$$

$$\frac{\partial P}{\partial y} = 0 \quad \text{at } y = 0 \text{ (Region II)} \tag{21}$$

$$\frac{\partial P}{\partial z} = 0 \quad \text{at } z = W_D/2 \text{ and } \text{L}_{IC} \leq x \leq \text{L}_T - 0.005\text{m}(\text{Region II}) \tag{22}$$

$$P = P_{atm} \quad \text{at } z = W_D/2 \text{ and } \text{L}_T - 0.005\text{m} < x \leq \text{L}_T(\text{Region II}) \tag{23}$$

$$\frac{\partial P}{\partial z} = 0 \quad \text{at } z = 0 \ (\text{Region II}) \tag{24}$$

$$\frac{\partial P}{\partial x} = 0 \quad \text{at } x = \text{L}_T \tag{25}$$

3.5 Finite Volume Method

The finite volume method [17] was used in this study to predict the pressure field, the velocity field, and the location and shape of the liquid resin flow front in the computational domain. In this method, the computational domain is divided into touching but non-overlapping finite control volumes (Fig. 5) which fill the domain, with one computational node associated with each control volume. The finite volume method approximates the partial differential equation over the control volume associated with the grid node. After applying the finite volume approach, discretization equations are obtained by integrating the partial differential equation for each control volume surrounding each grid node. Linear
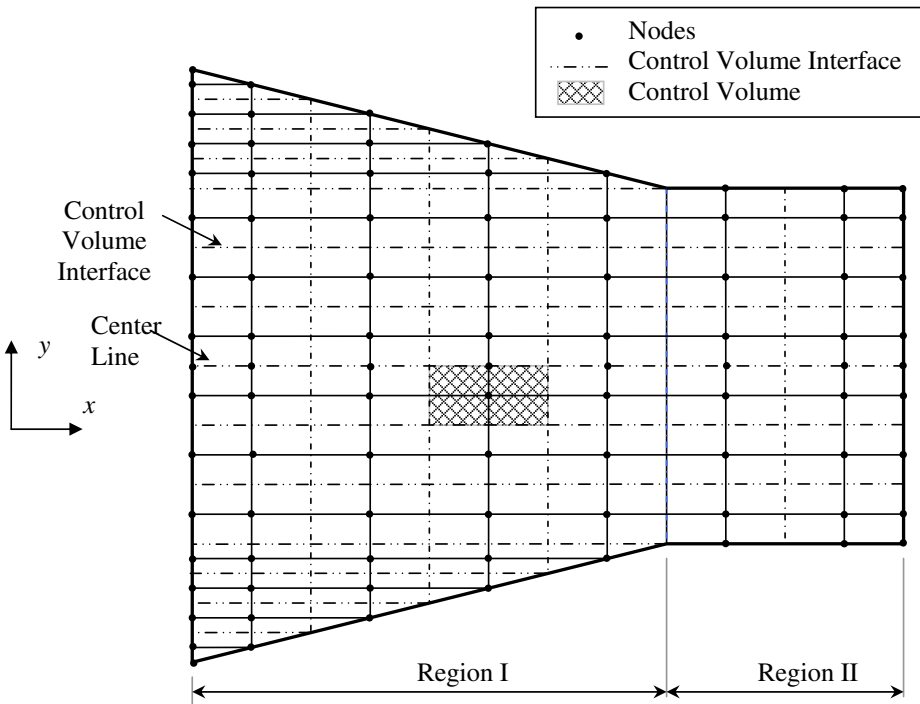

Fig. 5 Schematic of the computational domain

interpolation functions (or piecewise linear profile) expressing the variation of pressure between the grid points were used to evaluate the required integrals. The total number of quarter-domain computational nodes considered for modeling the injection chamber lengths of 0.15 m, 0.20 m, 0.30 m are 1302, 1722, and 2562, respectively. The computational grid was made progressively finer until the computational results became independent of grid fineness.

3.6 Solution of Algebraic Equations and Algorithm for Time Marching Scheme

To solve the governing pressure partial differential equations, (Eqs. 10 and 11), all the boundary conditions, initially based on velocity, were converted to pressure boundary conditions (Eqs. 12–25). The current solution technique employs the line-by-line tridiagonal matrix algorithm (TDMA-fully implicit technique) [17] to iteratively solve the system of discretized equations (pressure field) in the quarter-computational domain. Iterative methods are significant to handle non linearities and require much less computer storage to solve the system of discretized equations. The overall solution marches forward by a time-marching procedure.

After iteratively solving the pressure field at each time step, the velocity field was obtained by finite differencing of Darcy's [15] equations (Eq. 6). Details of the net mass flow rate of liquid resin into and out of the control volume was computed as presented in [18]. The domain was configured with a resin fill factor $F_{i,j,k}$ assigned to each control volume. $F_{i,j,k}$ is the fraction of the control volume occupied by liquid resin at a given time instant relative to the maximum liquid resin the control volume could hold. For a completely liquid filled control volume, the value of $F_{i,j,k}$ is unity (saturated reinforcement) and zero (dry reinforcement) if the control volume is empty of liquid. For each control volume, pressure was computed if it was fully saturated with liquid resin; otherwise, atmospheric pressure was assigned to it. Next the time steps needed to fill each of the remaining unfilled control volumes were determined. The minimum value of these time steps was the amount of time required to fill the next quickest-to-fill control volume, which had resin in it but was not yet completely filled, and yet not over-filling any other control volume. In this process of flow front advancement with time using this minimum time step approach, it was ensured that, at most, only one control volume was filled in one time step and no control volume was overfilled as time advanced forward. The fill factors of all unfilled or incompletely filled control volumes (where $0 \leq F_{i,j,k} < 1$) were updated at the end of each time step by using the minimum time step. In a given time step, the pultruded part was assigned to travel the length of the nodal control volume in the pull direction given by

$$0 < \Delta t_{\min} < \frac{L_{\min}}{U} \tag{26}$$

where L_{min} is the minimum length of the control volume in the pull speed direction and U is the fiber pull speed in the axial direction (x). Hence, the time step given in Eq. 26 was the default time step and time was not allowed to advance by an amount greater than given in this time step. No more than one control volume was allowed to be filled at each time step. This condition was checked at each time step. When the resin pressure field and liquid resin flow front did not change with time, the steady state was attained and no new control volumes were filled after this stage. The complete details of the time marching procedure are given in Ref. [18].

4 Results and Discussion

This work considers the impact of the processing parameters of pull speed (U), injection chamber length (L_T), and injection chamber compression ratio (CR) on the complete fiber reinforcement wet out, on the minimum resin injection pressure needed to achieve complete wet out, and importantly on the maximum resin pressure inside the injection chamber for different CR values of 2.0, 3.0 and 4.0. The simulations correspond to a composite consisting of fiberglass reinforcement with a phenolic resin system. Total lengths of the injection chamber (L_T) considered in this study are 0.15 m, 0.20 m and 0.30 m. Dual (one on top and one on bottom (see Figs. 2, 3 and 4)) injection slots of 0.010 m wide were investigated at two possible axial locations (x_{IS}) which were studied (40% or 60% downstream along the tapered lengths (L_{IC})) for L_T=0.15 m, 0.20 m and 0.30 m respectively. Simulations are carried out for fiber volume fraction and resin viscosity held fixed at the nominal values - - - nominal fiber volume fraction, V_{fo}=0.68, and nominal resin viscosity, μ=0.75 Pa.s.

The feasible criteria (constraints) for acceptable manufacturing solutions are: 1) an injection pressure to achieve complete wet out of not greater than 0.42 MPa (60 psi) and 2) a corresponding maximum interior chamber (exit) resin pressure (attached-die configuration) or maximum interior chamber resin pressure (detached-die configuration) of not greater than 1.72 MPa (250 psi). There were more acceptable manufacturing solutions for the proportional axial slot location of x_{IS}=0.60 L_{IC} than for the x_{IS}=0.40 L_{IC} location; whereas the general behaviors of the results are the same for both axial proportional locations [19]. Hence, all the discussions are presented for the axial injection slot location of x_{IS}=0.60 L_{IC} in this paper.

Figure 6 shows the resin pressure profiles for the nominal processing parameters (U= 0.0254 m/s, V_{fo}=0.68, μ=0.75 Pa.s) for CR=2.0, 3.0, 4.0 with chamber length of L_T= 0.30 m. For the detached-die (solid line) configuration, the injection chamber is separated from the heated pultrusion die (see Figs. 2, 3 and 4); whereas, for the attached-die (dashed line) configuration the injection chamber is not separated (Fig. 1) from the entrance to the heated pultrusion die. So the atmospheric pressure boundary conditions (Eqs. 20 and 23) apply to the circumference of the resin wetted fibers in the gap region for the detached-die configuration and thus there is a resin pressure relief occurring before entering the pultrusion die. Figure 6 shows how the atmospheric pressure boundary condition works in the detached-die configuration, in comparison to the attached-die configuration, to yield a lower maximum interior chamber wall pressure. The pressure difference (ΔP) between the maximum chamber wall pressure (detached) and the exit pressure (attached) is greater (see Table 1 and Fig. 7) as the injection chamber is made longer. Figure 6 also demonstrates that as CR increases, the maximum chamber wall pressure difference between the attached and detached configurations decreases. From Fig. 6 it is also clear that higher CR values yield lower interior injection chamber pressures.

Pull speed is an important processing parameter in pultrusion manufacturing to achieve high productivity. For high productivity, high pull speed is always desired without compromising the risk of exceeding the maximum resin injection pressure and maximum resin pressure constraints inside the injection chamber. Thus investigating the effect of the pull speed on minimum resin injection pressure to achieve complete wet out and the associated maximum chamber resin pressure is important. The simulation cases for the of pull speed impact on the minimum injection pressure to achieve complete wet out and maximum interior chamber pressure are presented in Table 1.

In Table 1, bold font indicates non-acceptable manufacturing solutions, not satisfying the following criteria: injection pressure ≤0.42 MPa (60 psi) and corresponding exit pressure

Fig. 6 Chamber wall axial
pressure profiles for detached
injection chamber and attached
injection chamber for L_T=0.30 m
for the nominal processing
parameters and x_{IS}=0.60 L_{IC}.
(H_D=0.0635 m,
W_D=0.00318 m).
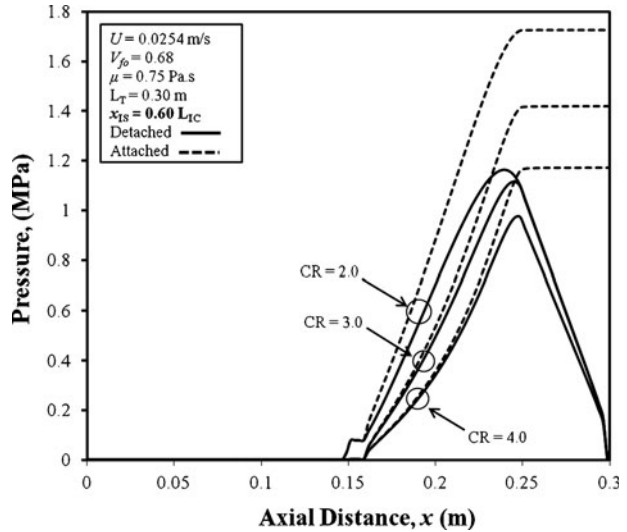
(attached configuration) or maximum wall pressure (detached configuration) ≤1.72 MPa (250 psi). The higher the pull speed, the higher the injection pressure required to achieve complete reinforcement wet out and hence the higher the corresponding maximum interior chamber pressure. Higher pull speeds increase the maximum chamber wall pressure because the resin is more rapidly compressed. For a CR value of 2.0, as the pull speed increases, the injection pressure necessary for the complete wet out increases due to the increased sweeping away of the liquid resin at the resin injection slot by the fiber reinforcement. But for CR values of 3.0 and 4.0, the injection pressure necessary for complete wet out has a constant value of about 0.002 MPa (15 psi). This is due to the quite low local fiber volume fraction ($V_f(x)$) at the resin injection slot for these higher CR values which easily allows the flow of the liquid resin through the fiber reinforcement.

Figure 7 shows the pull speed impact on pressure for CR=4.0 for chamber lengths of 0.15 m, 0.20 m, and 0.30 m. The lower horizontal dotted line (0.42 MPa) and the upper dotted horizontal line (1.72 MPa) represent the pressure limits for the acceptable manufacturing solutions for the resin injection pressure and the maximum chamber wall resin pressure, respectively. The longer the length of the injection chamber, the higher is the maximum chamber wall pressure. The higher maximum chamber wall pressure is the result of the pressure rise due to the source term in Eq. 10 which occurs as a result of tapering the walls of the injection chamber; the maximum chamber pressure increases as L_T increases due to the longer distance over which the resin is compressed. Because of this, it can be seen in Fig. 7 that for the highest pull speed of 0.0508 m/s, the maximum chamber pressure occurs in the non-feasible manufacturing region (>1.72 MPa) for large L_T values. As the pull speed increases the maximum chamber pressure also increases due to rapid compressing of the liquid resin by the rapid increasing of the local fiber volume fraction along the chamber length. Comparison of the maximum chamber pressure between the attached-die configuration and detached-die configuration is illustrated in Fig. 7. It can be observed that the maximum chamber pressure is always lower for the detached-die configuration and for the lower pull speed; the maximum chamber pressure difference between the two configurations (attached versus detached) increases as the pull speed increases.

Table 1 Effect of pull speed, U, on minimum injection pressure necessary to achieve complete wet out for different processing parameters for slot width=0.01 m, part width=0.0635 m, part thickness=0.00318 m at a proportional slot location x_{IS}=0.60 L_{IC}

| Case	CR	U (m/s)	V_{fo}	μ Pa.s	Injection pressure (Gauge) (MPa)	Total length L_T (m)	Location of x_{IS} (m)	Exit pressure (Gauge) (MPa) (Attached)	Maximum chamber pressure (Gauge) (MPa) (Detached)
A1	2.0	0.0203	0.68	0.75	0.057	0.15	0.06	0.525	0.475
A2	2.0	0.0254	0.68	0.75	0.071	0.15	0.06	0.656	0.570
A3	2.0	0.0508	0.68	0.75	0.147	0.15	0.06	1.347	1.150
B1	3.0	0.0203	0.68	0.75	0.002	0.15	0.06	0.454	0.415
B2	3.0	0.0254	0.68	0.75	0.002	0.15	0.06	0.570	0.520
B3	3.0	0.0508	0.68	0.75	0.002	0.15	0.06	1.136	1.040
C1	4.0	0.0203	0.68	0.75	0.002	0.15	0.06	0.380	0.361
C2	4.0	0.0254	0.68	0.75	0.002	0.15	0.06	0.474	0.413
C3	4.0	0.0508	0.68	0.75	0.002	0.15	0.06	0.950	0.830
D1	2.0	0.0203	0.68	0.75	0.057	0.20	0.09	0.677	0.576
D2	2.0	0.0254	0.68	0.75	0.078	0.20	0.09	0.880	0.715
D3	2.0	0.0508	0.68	0.75	0.147	0.20	0.09	1.700	1.375
E1	3.0	0.0203	0.68	0.75	0.002	0.20	0.09	0.560	0.475
E2	3.0	0.0254	0.68	0.75	0.002	0.20	0.09	0.700	0.590
E3	3.0	0.0508	0.68	0.75	0.002	0.20	0.09	1.400	1.190
F1	4.0	0.0203	0.68	0.75	0.002	0.20	0.09	0.450	0.400
F2	4.0	0.0254	0.68	0.75	0.002	0.20	0.09	0.561	0.501
F3	4.0	0.0508	0.68	0.75	0.002	0.20	0.09	1.122	1.000
G1	2.0	0.0203	0.68	0.75	0.064	0.30	0.15	1.380	0.968
G2*	2.0	0.0254	0.68	0.75	0.078	0.30	0.15	1.727	1.198
G3*	2.0	0.0508	0.68	0.75	0.133	0.30	0.15	3.393	2.390
H1	3.0	0.0203	0.68	0.75	0.002	0.30	0.15	1.135	0.890
H2	3.0	0.0254	0.68	0.75	0.002	0.30	0.15	1.420	1.120
H3*	3.0	0.0508	0.68	0.75	0.002	0.30	0.15	2.840	2.230
I1	4.0	0.0203	0.68	0.75	0.002	0.30	0.15	0.936	0.786
I2	4.0	0.0254	0.68	0.75	0.002	0.30	0.15	1.171	0.984
I3*	4.0	0.0508	0.68	0.75	0.002	0.30	0.15	2.342	1.960

*Bold font indicates non-acceptable manufacturing solutions, not satisfying the following criteria:

injection pressure ≤0.42 MPa (60 psi) and corresponding exit pressure (attached configuration) or maximum wall pressure (detached configuration) ≤1.72 MPa (250 psi)

Figure 8 demonstrates the minimum injection pressure to achieve complete wet out and the corresponding maximum chamber pressure variations for different CR values at the highest pull speeds of U=0.0508 m/s. As the CR value increases the maximum chamber pressure also decreases due to the larger taper angle (α). All the attached-die configuration curves and detached-die configuration curves show the same qualitative behavior as in Fig. 7, but the attached-die configuration curves have greater curvature due to the higher rise in maximum chamber pressure as the injection chamber length increases. For the highest pull speed of 0.0508 m/s (Fig. 8), the more favorable manufacturing solutions for an acceptable chamber wall pressure are the detached-die configurations with a CR value of 4.0 and an injection chamber length of L_T≤0.28 m.

Figure 9 shows the resin flow front profile through the fiber reinforcement for a favorable manufacturing solution with an injection chamber length of 0.15 m and CR=4.0 for the

Fig. 7 Maximum wall pressure (——) for detached injection chamber and exit wall (maximum) pressure (———) for attached injection chamber vs. chamber length for CR=4.0, (H_D=0.0635 m, W_D=0.00318 m); minimum injection pressure (—·—) to achieve complete wet out
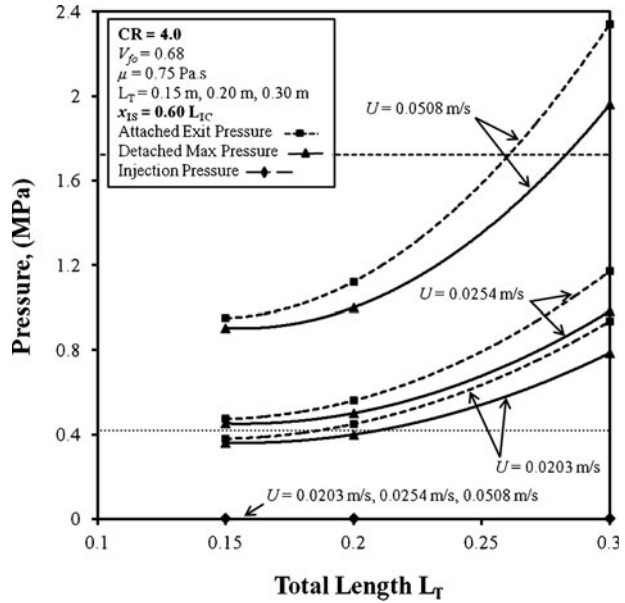
highest pull speed of 0.0508 m/s considered and other nominal processing parameters (V_{fo}= 0.68 and μ=0.75 Pa.s). The white portion inside the injection chamber corresponds to dry fiber and the shaded region corresponds to the liquid resin and fiber mixture. The thick dark line corresponds to the resin flow front of the resin/fiber system and the thin lines illustrate the isopressure contours labeled with pressure values in kPa. The resin flow front and the pressure values for the attached-die configuration and the detached-die configuration can be compared in these two figures. The chamber pressure values are always lower in the detached-die configuration system as compared to the attached-die configuration shown in

Fig. 8 Maximum wall pressure (——) for detached injection chamber and exit wall (maximum) pressure (———) for attached injection chamber vs. chamber length for various CR, (H_D=0.0635 m, W_D= 0.00318 m); minimum injection pressure (—·—) to achieve complete wet out

a.   Die-Attached Configuration

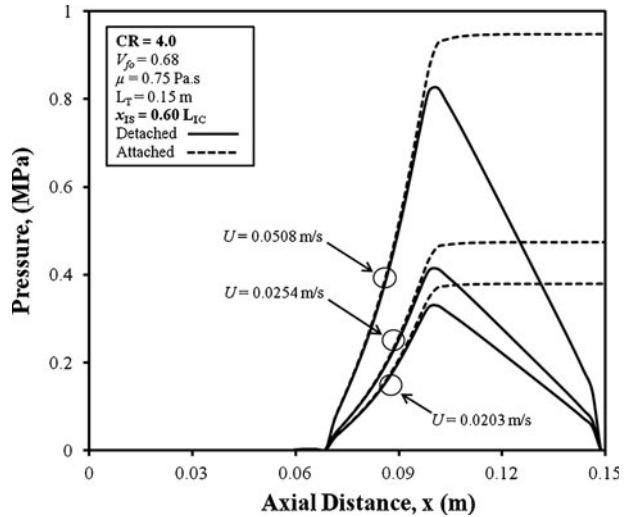b.   Die-Detached Configuration
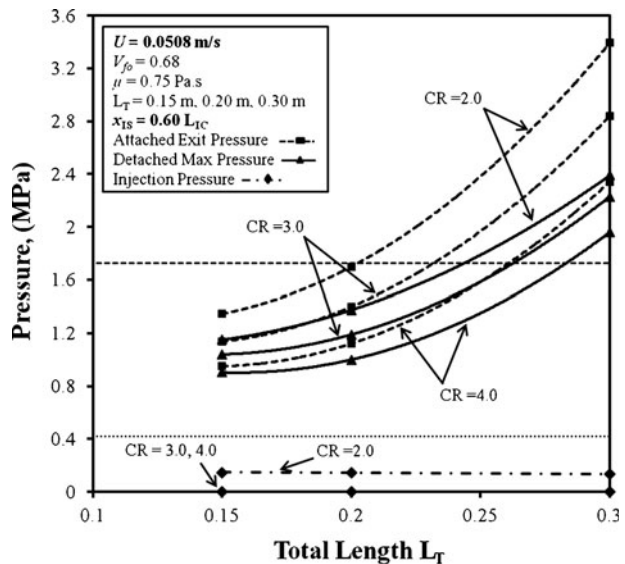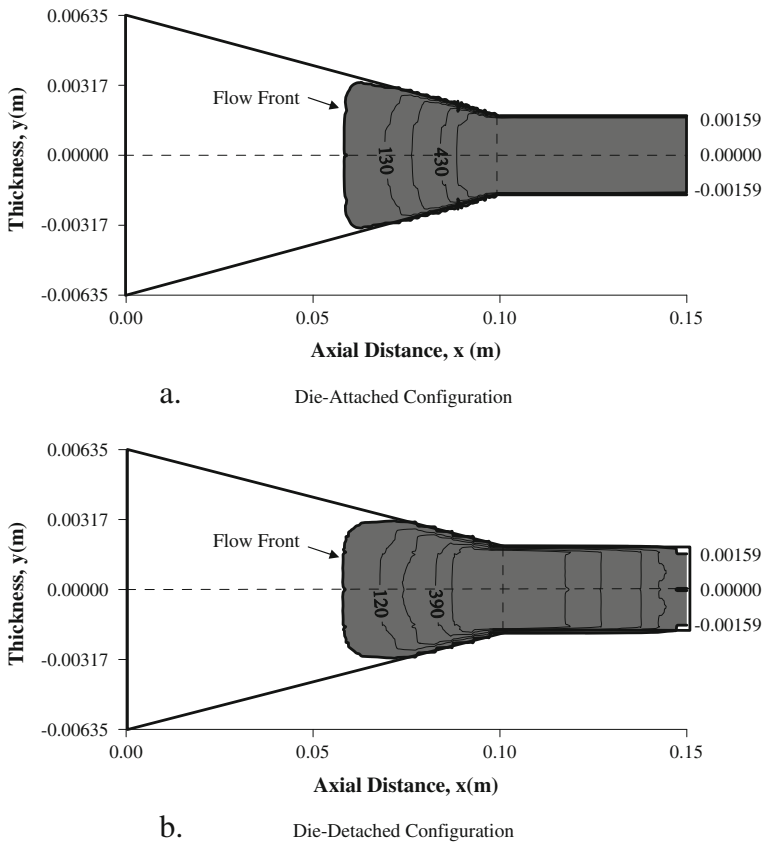
Fig. 9 Flow front profile and gauge isopressure (kPa) contours for case C3, Table 4–3 with $U=0.0508$ m/s for polyester resin/glass roving, $L_T=0.15$ m, CR=4.0, $V_{fo}=0.68$ and $\mu=0.75$, $x_{IS}=0.60$ L_{IC} (not to scale)

Fig. 9. In the detached-die configuration, the isopressure contours can be seen in Region II of the injection chamber due to the decreasing chamber pressure in the Region II. Figure 9 is not made to scale to make it more viewable to the reader.

Figure 10 depicts the chamber wall pressure profiles along the interior length of the injection chamber for $L_T=0.15$ m and for CR=4.0. This figure illustrates the chamber wall pressure profile progression inside the injection chamber for both the attached-die and detached-die configurations and thus this figure illustrates the difference in the pressure profile development for these two (attached versus detached) configurations as a function of pull speed. Figure 11 demonstrates the pressure profiles in the detached-die configuration for all the chamber lengths considered at the highest pull speed considered of $U=0.0508$ m/s. Figure 11 shows the broad spectrum of pressure profiles for the detached-die configuration for different CR values depicting how the pressure increases and then decreases back to the atmospheric pressure (in the gap) beyond the injection chamber exit. For lower pull speeds, it is easier to control the process and achieve complete wet out and the corresponding maximum chamber pressure is also lower. For the pull speed of 0.0508 m/s, the lowest acceptable maximum chamber pressure is obtained for a chamber length of 0.15 m and CR= 4.0. Thus, when very high pull speed is desired (0.0508 m/s in this work), a short chamber length of 0.15 m and high CR value of 4.0 is required to have an acceptable pultrusion

Fig. 10 Chamber wall axial pressure profiles for detached injection chamber and attached injection chamber for chamber length of 0.15 m for CR=4.0, (H_D=0.0635 m, W_D=0.00318 m)

manufacturing solution which satisfies the pressure constraints on both injection pressure and maximum interior chamber pressure. Lower maximum chamber pressures are obtained by employing the detached-die configuration; hence, as a result the detached-die configuration is a better choice for pultrusion manufacturing than the attached-die configuration.

5 Conclusions

This study is focused on the impact of pull speed, compression ratio, and injection chamber length on the minimum injection pressure required for complete wet out and the associated maximum chamber wall pressure for both the attached-die and detached-die configurations. For this a 3D finite volume method was applied to model the flow of liquid resin through the

Fig. 11 Chamber wall axial pressure profiles of detached injection chamber for different chamber lengths of 0.15 m, 0.20 m and 0.30 m for U=0.0508 m/s, (H_D=0.0635 m, W_D=0.00318 m)
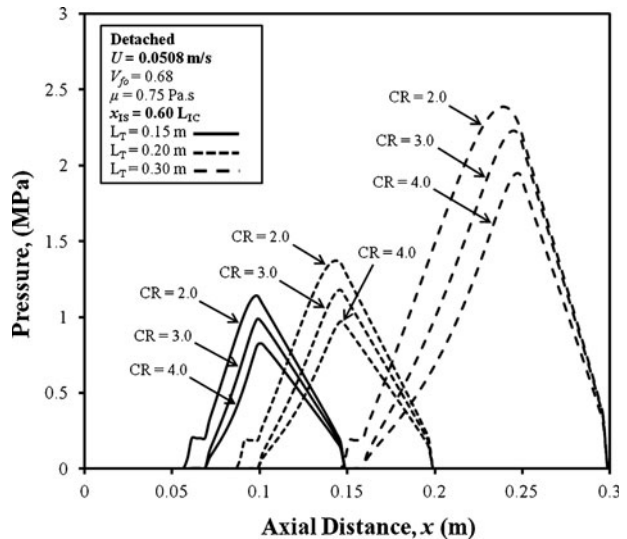
fiber reinforcement in the resin injection pultrusion manufacturing process. Practical pressure limits criteria were set for successful manufacturing solutions; the minimum injection pressure for complete wet out should be below 0.42 MPa (60 psi or about 4 atmospheres) and the corresponding maximum chamber wall pressure should be below 1.72 MPa (250 psi or about 16.5 atmospheres). The general behaviors of the maximum chamber wall pressure (Fig. 7) for different pull speeds with respect to injection chamber length were trend wise similar and non-linearly increasing for both the attached-die and detached-die configurations. For higher CR values the local fiber volume fraction at the injection slot location is lower which decreases the resistance to the resin flow into fiber and this plays a significant role in the injection pressure requirement to achieve complete wet out. Thus higher injection pressure values are required for CR value of 2.0; whereas, for CR value of 3.0 and 4.0, the injection pressure of 0.002 MPa gauge pressure (slightly greater than atmospheric pressure) is sufficient for complete fiber wet out and the processing parameters have no effect on the minimum injection pressure required for complete fiber wet out. When very high pull speed is desired (0.0508 m/s in this work), a short injection chamber length of 0.15 m and high CR value of 4.0 is recommended to have an acceptable pultrusion manufacturing solution. This work concludes that the manufacturing solution for resin injection pultrusion is the detached-die configuration with a short injection chamber length and high CR value for providing favorable operating conditions for the pultrusion manufacturing process of composite materials.

References

1. Jeswani, J.L., Roux, J.A.: Numerical modeling of design parameters for manufacturing polyester/glass composites by resin injection pultrusion. Polym. Polym. Compos. **14**(7), 651–669 (2006)
2. Lackey, E., Vaughan, J.G., Roux, J.A.: Experimental development and evaluation of a resin injection system for pultrusion. J. Adv. Mater. **29**, 30–37 (1997)
3. Rahatekar, S.S., Roux, J.A.: Numerical simulation of pressure variation and resin flow in injection pultrusion. J. Compos. Mater. **37**(12), 1067–1082 (2003)
4. Sharma, D., McCarty, T.A., Roux, J.A., Vaughan, J.G.: Investigation of dynamic behavior in a pultrusion die. J. Compos. Mater. **32**(10), 929–950 (1998)
5. Ranga, B.K.: Impact of chamber length on performance of tapered resin injection pultrusion. Masters Thesis, University of Mississippi (2009)
6. Srinivasagupta, D., Kardos, J.L.: Rigorous dynamic model-based economic design of the injected pultrusion process with controllability considerations. J. Compos. Mater. **37**(20), 1851–1888 (2003)
7. Srinivasagupta, D., Potaraju, S., Kardos, J.L., Joseph, B.: Steady state and dynamic analysis of a bench-scale injected pultrusion process. Compos. Appl. Sci. Manuf. **34**, 835–846 (2003)
8. Mustafa, I., Khomami, B., Kardos, J.L.: 3-D Nonisothermal flow simulation model for injected pultrusion processes. AICHE J. **45**(1), 151–163 (1999)
9. Dube, M.G., Batch, G.L., Vogel, J.H., Mocosko, C.W.: Reaction injection pultrusion of thermoplastic and thermoset composites. Polym. Compos. **16**, 378–385 (1995)
10. Li, S., Xu, L., Ding, Z., Lee, L.J.: Experimental and theoretical analysis of pulling force in pultrusion and resin injection pultrusion (RIP) – part I: experimental. J. Compos. Mater. **37**(3), 163–189 (2003)
11. Li, S., Xu, L., Ding, Z., Lee, L.J.: Experimental and theoretical analysis of pulling force in pultrusion and resin injection pultrusion (RIP) – Part II: modeling and simulation. J. Compos. Mater. **37**(3), 195–216 (2003)
12. Liu, X.L.: A finite element/nodal volume technique for flow simulation of injection pultrusion. Composites: Part A **34**, 649–661 (2003)
13. Liu, X.L.: Iterative and transient numerical models for flow simulation of injection pultrusion. Compos. Struct. **66**(1–4), 175–181 (2003)
14. Gutowski, T.G., Cai, A., Bauer, S., Boucher, D., Kingery, J., Wineman, S.: Consolidation experiments for laminate composites. J. Compos. Mater. **21**, 650–669 (1987)
15. Carman, P.C.: Fluid flow through granular beds. Trans. Int. Chem. Eng. **5**, 150–166 (1937)

16. Darcy, H.: Les fontaines publique de la ville de Dijon. Dalmont, Paris (1856)
17. Patankar, S.: Numerical Heat Transfer and Fluid Flow. Hemisphere Publishing Corporation, New York (1980)
18. Jeswani, A.: 3-D Numerical modeling of injection pultrusion process. PhD Thesis, University of Mississippi (2006)
19. Palikhel, D.R.: Processing parameters and injection chamber length impact on resin injection pultrusion. Masters Thesis, University of Mississippi (2011)